Supplementary Data

Enhanced Myelination with Concomitant Ultrastructural Irregularities following Prenatal Exposure to Ambient Particulate Matter in the Mouse

Carolyn Klocke, Valeriia Sherina, Uschi M. Graham, Jakob Gunderson, Joshua L. Allen, Marissa Sobolewski, Jason L. Blum, Judith T. Zelikoff, and Deborah A. Cory-Slechta

Supplementary methods

Transmission electron microscopy (TEM) and ultrastructural myelin measurements

Tissue was prepared for high-resolution EM as described in Materials and Methods. Myelin *g*-ratio and myelin sheath integrity scores were determined using ImageJ software (National Institutes of Health, Bethesda, MD) by a blinded experimenter.

For preliminary *g*-ratio analysis, axons selected for analysis (N = 100 axons/sample) were sampled from ≥ 3 fields in the midbody of the CC and had the appearance of completed myelination, i.e. complete myelin wrapping without delamination or damage. Selected axons were of varying diameters to assess whether myelination status was consistent across axons of different caliber. Cross-sectional axonal area was determined by hand-tracing the circumference of each axon without measuring myelin, and then again with the inclusion of the myelin sheath (myelinated axonal area). Axonal diameter (with and without myelin) was mathematically derived from each area measurement to prevent bias and *g*-ratio was calculated as follows: $g = d_i/d_o$, where d_i = inner axon diameter (also referred to as axon caliber) and d_o = diameter of axon plus myelin, i.e. outer myelinated diameter.

Myelin integrity scoring was determined for a minimum of 100 axons in 3 fields using ImageJ. Each stage of myelination was scored using a numeric designation as follows: (1) unmyelinated axons, (2) partially myelinated axons, (3) completely myelinated axons with intact myelin, and (4) completely myelinated axons with damage. This scoring paradigm allowed the quantification of axons within each field (one field = ~696.8 μm^2). The average total axons per field is reported in **Figure S2d**.

Statistical analyses for EM experiments

Statistical analyses were conducted using JMP Pro 12.0 (SAS Institute Inc., Cary, NC). Myelin thickness, axon caliber, myelin *g*-ratio, myelin integrity scoring, and axon quantification were analyzed separately by sex or exposure via one-way ANOVA. Sexes were compared within exposure groups to determine any incidence of sex-specific effects. Linear regression and correlation analyses of both *g*-ratio and myelin thickness vs. axon caliber were performed with exposure group (CAPs or Air), axon caliber, and sex as between-group factors. Due to the limited sample size and exploratory nature of ultrastructural assessments, *post hoc* analyses for multiple comparisons were not performed. The tissue section/visual field was the experimental unit (i.e. replicate) for measures of myelin sheath thickness, *g*-ratio, axon caliber, myelin integrity scoring, and axon quantification. For correlative and linear regression analyses, each axon measurement was plotted individually. *P*-values ≤ 0.05 were considered statistically significant.

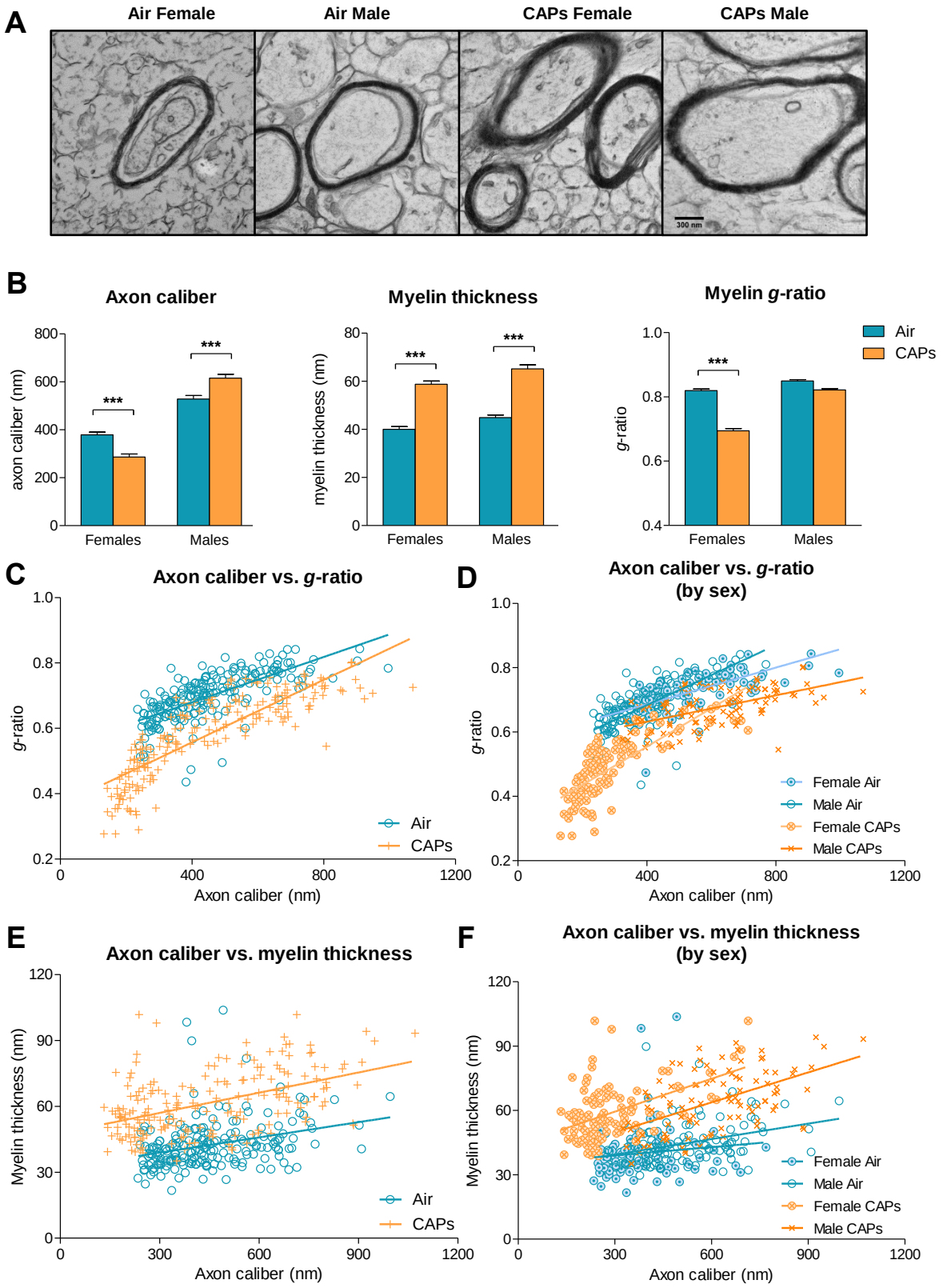

Figure S1: Gestational CAPs exposure alters the trajectory of corpus callosum (CC) axon caliber, myelin thickness, and *g*-ratio at PND12. (Legend on following page.)

Figure S1 (continued): Tissue from the midbody CC was prepared for electron microscopy (EM) and imaged. Axon caliber (i.e. diameter) and myelin thickness were determined using ImageJ and used to calculate *g*-ratio. **A)** Representative images from each exposure group. Scale bar represents 300 nm. **B)** CAPs exposure altered axon caliber in a sex-specific manner. Myelin thickness was increased in both sexes as a result of gestational CAPs exposure with a corresponding decrease in *g*-ratio in CAPs-exposed females. Data represent mean ± SEM of 100 axons per animal imaged in at least 3 fields (N = 1 animal/sex/exposure). Statistical outcome: ***$p < 0.0001$. **C-D)** The correlative relationship of axon caliber and *g*-ratio was affected by prenatal CAPs exposure ($F_{3,399} = 352.8$, $p < 0.0001$). This linear relationship was significantly sex-specific ($p = 0.001$); therefore, sexes are combined in **C** (Air: $r^2 = .69$, $p < 0.0001$; CAPs: $r^2 = 0.83$, $p < 0.0001$; N = 2 animals/exposure) and separate in **D** (Air female: $r^2 = 0.66$, $p < 0.0001$; Air male: $r^2 = 0.66$, $p < 0.0001$; CAPs female: $r^2 = 0.74$, $p < 0.0001$; CAPs male: $r^2 = 0.55$, $p < 0.0001$; N = 1 animal/sex/exposure). Data represent 100 axons per animal imaged in ≥ 3 fields. **E-F)** The correlative relationship of axon caliber and myelin sheath thickness was affected by prenatal CAPs exposure ($F_{3,399} = 116.7$, $p < 0.0001$). This linear relationship was sex-specific with trending significance ($p = 0.09$); therefore, sexes are combined in **E** (Air: $r^2 = 0.31$, $p < 0.0001$; CAPs: $r^2 = 0.48$, $p < 0.0001$; N = 2 animals/exposure) and separate in **F** (Air female: $r^2 = 0.13$, $p = 0.21$; Air male: $r^2 = 0.34$, $p = 0.0004$; CAPs female: $r^2 = 0.48$, $p < 0.0001$; CAPs male: $r^2 = 0.51$, $p < 0.0001$; N = 1 animal/sex/exposure).

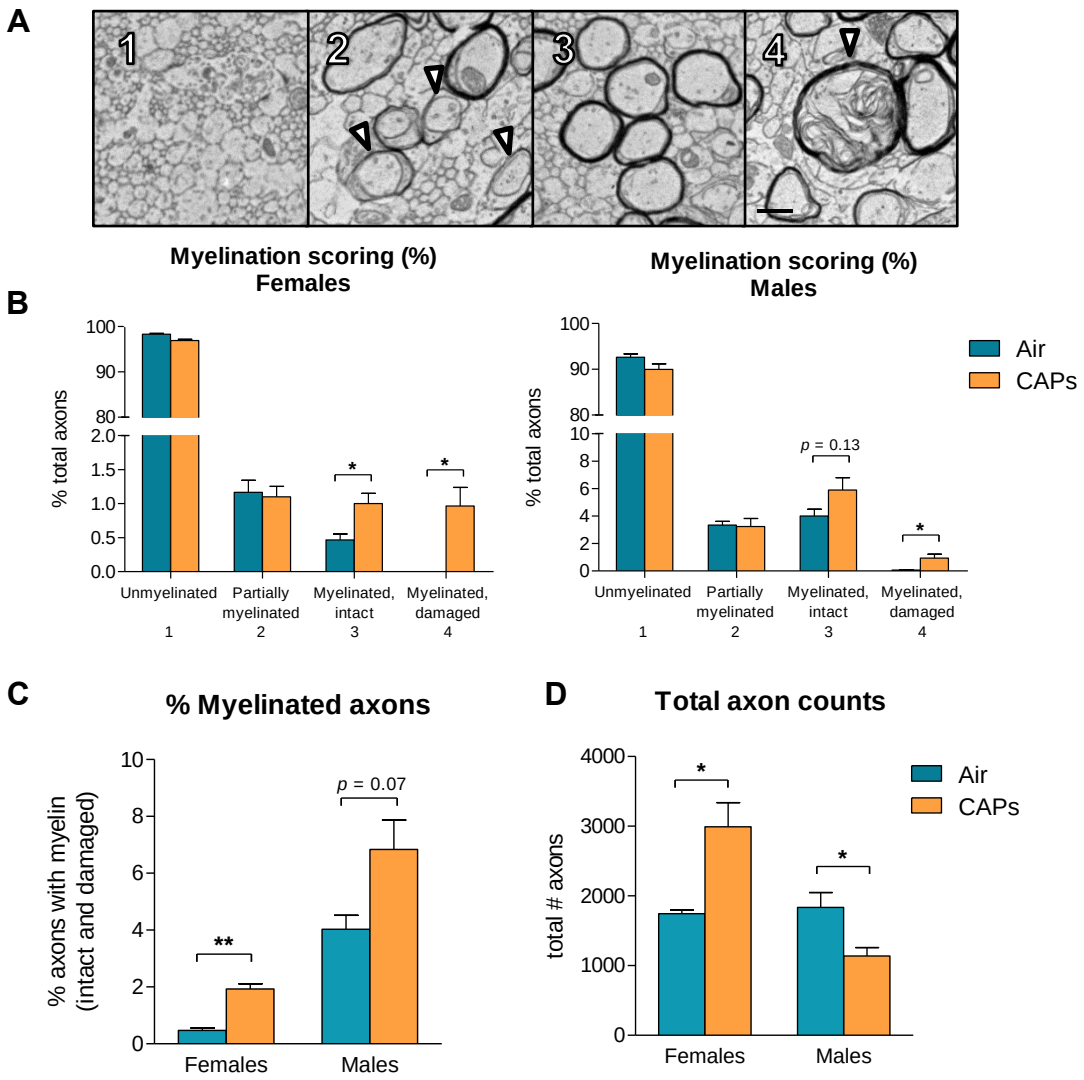

Figure S2: The proportion of myelinated axons and axons with myelin damage and/or malformation is elevated at PND12 following gestational exposure to CAPs. Following prior observations that myelin sheaths were damaged when imaged via high-resolution scanning transmission EM (HRSTEM), the proportion of myelinated/damaged axons (i.e. myelin sheath integrity) in the CC was determined in a separate group of animals. Tissue from the midbody CC was prepared for transmission EM, imaged, and all axons were scored/quantified in 3 separate fields using ImageJ. Scale bar represents 300 nm. **A)** Representative transmission electron micrographs of each stage of myelination scored from a CAPs-exposed male: (1) unmyelinated axons, (2) partially myelinated axons, (3) completely myelinated axons with intact myelin, and (4) completely myelinated axons with damage/evidence of malformation. **B)** Prenatal CAPs exposure increases the proportion of myelinated, intact and myelinated, damaged axons relative to Air controls in females and males. **C)** When analyzed together, the total proportion of axons with complete myelination (intact and damaged) is elevated in both CAPs-exposed females and males. **D)** The total number of axons enumerated in 3 separate fields was elevated in CAPs-exposed females and decreased in CAPs-exposed males. Data represent mean ± SEM of 3 fields (N = 1 animal/sex/exposure). Statistical outcome: *$p < 0.05$, **$p < 0.01$.

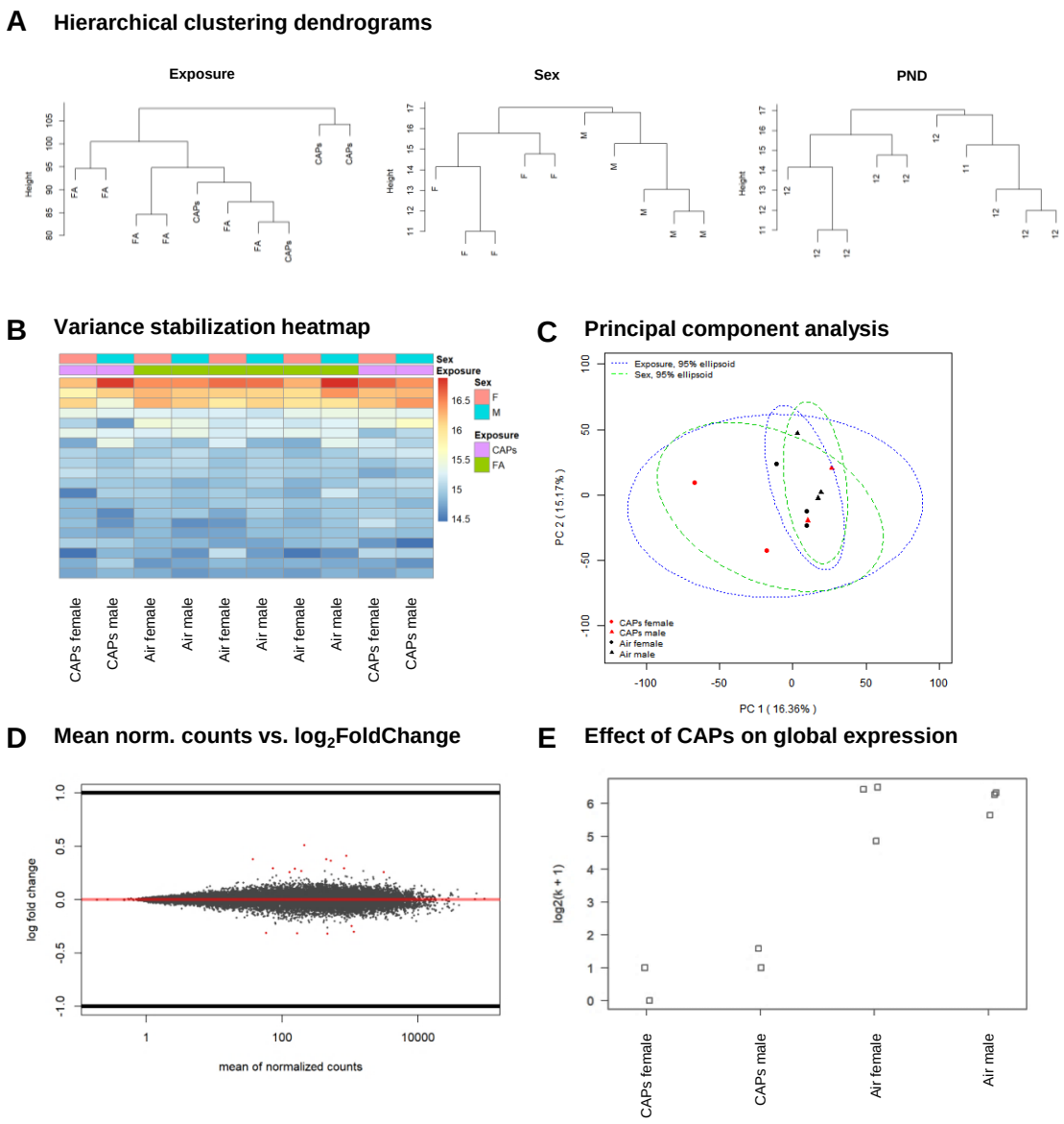

Figure S3: Gestational CAPs exposure significantly alters global mRNA expression in males and females at PNDs 11-12. Dissected, frozen cerebellum tissue from PNDs 11-12 was processed for RNAseq and analyzed using Bioconductor software in R. **A)** Hierarchical clustering analyses of exposure, PND, and sex. PND13 was significantly different than PNDs 11-12 (not shown), although there was no difference between PNDs 11 and 12. Thus, both PND11 and PND12 are included in analyses and PND13 is excluded. **B)** Heatmap of variance-stabilized differential gene expression. **C)** Principal component analysis of gene expression for PNDs 11 and 12 revealed no significant clustering of samples around any single factor. Ellipses indicate 95% confidence intervals for exposure (blue, dotted) and sex (green, dashed). **D)** Comparison of mean normalized gene expression counts vs. log-transformed fold change gene expression. Red points indicate statistically significant differential expression (p-adj. ≤ 0.05). **E)** Strip chart depicting overall differential gene expression between CAPs- and Air-exposed offspring (Air group indicated by 'FA'). Data represent N = 2-3/sex/exposure. Statistical outcome: p-value of log-normalized data adjusted for sex, PND, and false discovery rate < 0.05.

Table S1: Significantly differentially expressed genes with documented neurological/neurodevelopmental associations

Gene symbol	Gene name	Type of molecule encoded	Directionality of prenatal CAPs effect	Reference	Species	Findings
Sox2ot	SRY (sex determining region Y)-box 2 overlapping transcript	lncRNA	Upregulated	Arisi et al. (2011)	Mouse	Increased expression suggested as a biomarker of neurodegenerative disease
				Amaral et al. (2009)	Zebrafish	Constitutively expressed in areas of active neurogenesis; possible enhancer of neurogenesis in forebrain
Pcsk9	Proprotein convertase subtilisin/kexin type 9	Protein	Upregulated	Seidah et al. (2003)	Mouse	Expression is enhanced in proliferating CGNs from E15 through PND15
				Rousselet et al. (2011)	Mouse	Negative regulator of cholesterol homeostasis in external granule layer of the cerebellum at PND7; expression is enhanced during neurodevelopment
				Kysenius et al. (2012)	Mouse	RNAi knockdown reduced neuronal apoptosis in *ex vivo* CGN cultures
				Poirier et al. (2006)	Zebrafish	Regulator of neuronal differentiation; global knockdown resulted in cerebellar disorganization and embryonic death
Exosc9	Exosome component 9	Protein	Upregulated	Donkervoort et al. (2017)	Human	Homozygous recessive mutation produced cerebellar hypoplasia, hypomyelination in human infants
				Arteta et al. (2016)	Human	Increased expression in frontal cortex of individuals with severe depression
Capza1	F-Actin-capping protein subunit alpha-1	Protein	Upregulated	Taoka et al. (1992)	Rat	Cerebellar expression transiently increased at PND7
Zfhx2os	Zinc finger homeobox 2, opposite strand	ncRNA	Downregulated	Komine et al. (2006)	Mouse	Enhanced expression in PND8 cerebellum correlates with and negatively regulates *Zfhx2* mRNA expression
				Komine et al. (2012)	Mouse	*Zfhx2*-null mice presented with neurobehavioral deficits without neuroanatomical alterations
Gas5	Growth arrest-specific 5	lncRNA	Downregulated	Meier et al. (2010)	Mouse	Elevated hippocampal expression observed with associated memory impairments at advanced age

Gene symbol	Gene name	Type of molecule encoded	Directionality of prenatal CAPs effect	Reference	Species	Findings
				Sun et al. (2017)	Mouse	Suppressor of microglial M2 polarization; microglial knockdown promotes OPC survival and attenuates demyelination following EAE
				Caldwell et al. (2018)	Mouse	Prenatal As exposure induced sex-specific reductions at GD16 and GD18 in male offspring brain with corresponding reduction in GR; female offspring unaffected
				Zhao et al. (2018)	Rat	Significantly upregulated following neonatal hypoxic/ischemic brain injury; silencing was protective
Kcnmb2	Potassium large conductance calcium-activated channel, subfamily M, beta member 2	Protein	Downregulated	Katsumata et al. (2017)	Human	Allelic variants associated with significantly increased risk of AD
Slc39a2	Solute carrier family 39	Protein	Downregulated	Peters et al. (2007)	Mouse	Global knockout reduced embryonic Fe uptake in maternal dietary Fe overload conditions
				Liuzzi et al. (2005)	Mouse	mRNA expression decreases in response to inflammatory stimuli
				Ament et al. (2015)	Human	Disrupting mutations observed in individuals with hereditary bipolar disorder
Pabpn1	Polyadenylate-binding protein 2	Protein	Downregulated	Messaed et al. (2007)	Human	Allelic variant with trinucleotide repeats underlies oculopharyngeal muscular dystrophy
				Dion et al. (2005)	Mouse	Transgenic mice expressing expanded variant exhibit neuromotor deficits and neurodegeneration
				Chou et al. (2015)	Drosophila	Reduced expression resulted in enhanced ALS-like phenotype and disease progression
1500004A13Rik	RIKEN cDNA 1500004A13 gene	ncRNA	Upregulated	Iacono et al. (2017)	Mouse	OL-specific enhanced expression occurs during perinatal development periods
Olfml2b	Olfactomedin-like 2B	Protein	Upregulated	Langerveld et al. (2007)	Human	Elevated expression observed in rostral pons tissue of patients with multiple system atrophy

Gene symbol	Gene name	Type of molecule encoded	Directionality of prenatal CAPs effect	Reference	Species	Findings
				Lencz et al. (2010)	Human	Suggested schizophrenia risk factor gene
				Martin et al. (2014)	Human	Copy number variant reported as a risk factor for ASD and ADHD
Rpl21	Ribosomal protein L21	Protein	Upregulated	Tajouri et al. (2003)	Human	Elevated expression observed in acute demyelinating lesions of patients with MS
				Riva et al. (2016)	Human	Significant enrichment observed in motor nerves of patients with ALS
				Garcia-Esparcia et al. (2017)	Human	Significant upregulation in brain tissue of patients with AD
				Rafalski et al. (2013)	Mouse	Elevated expression in SIRT1-null mice corresponds with expansion of OPCs and myelinating OLs
				Padhi et al. (2008)	Rat	Elevated expression in female cerebellum after prenatal and perinatal exposure to organlochlorine pesticides
Fcrls	Fc receptor-like S, scavenger receptor	Protein	Upregulated	Parente et al. (2012)	Mouse	Increased expression observed in cerebellum of mice with lysosomal storage disorder
				Butovsky et al. (2014)	Mouse	Significantly enriched in microglia compared to macrophages

AD = Alzheimer's disease, ADHD = attention deficit hyperactivity disorder, ALS = amyotrophic lateral sclerosis, As = arsenic, ASD = autism spectrum disorder, CGN = cerebellar granule neuron, EAE = experimental autoimmune encephalomyelitis, Fe = iron, GR = glucocorticoid receptor, lncRNA = long noncoding RNA, MS = multiple sclerosis, ncRNA = noncoding RNA, OL = oligodendrocyte, OPC = oligodendrocyte progenitor cell

No known neurological associations were found for the following significantly differentially expressed genes: *Gm5148*, *RP23-111M12.3*.

Supplementary References

Amaral, P.P., et al., 2009. Complex architecture and regulated expression of the Sox2ot locus during vertebrate development. RNA 15(11), 2013-2027.

Ament, S.A., et al., 2015. Rare variants in neuronal excitability genes influence risk for bipolar disorder. Proc. Natl. Acad. Sci. U. S. A. 112(11), 3576-3581.

Arisi, I., et al., 2011. Gene expression biomarkers in the brain of a mouse model for Alzheimer's disease: mining of microarray data by logic classification and feature selection. J. Alzheimers Dis. 24(4), 721-738.

Arteta, D., et al., 2016. Transgenic animal model of mood disorders, in: Office, U.S.P.a.T. (Ed.). Brainco Biopharma SL

Butovsky, O., et al., 2014. Identification of a unique TGF-β–dependent molecular and functional signature in microglia. Nat. Neurosci. 17(1), 131.

Caldwell, K.K., et al., 2018. Arsenic exposure during embryonic development alters the expression of the long noncoding RNA growth arrest specific-5 (Gas5) in a sex-dependent manner. Neurotoxicol. Teratol. 66, 102-112.

Chou, C.C., et al., 2015. PABPN1 suppresses TDP-43 toxicity in ALS disease models. Hum. Mol. Genet. 24(18), 5154-5173.

Dion, P., et al., 2005. Transgenic expression of an expanded (GCG)13 repeat PABPN1 leads to weakness and coordination defects in mice. Neurobiol. Dis. 18(3), 528-536.

Donkervoort, S., et al., 2017. Recessive mutation in EXOSC9 disrupts the exosome complex resulting in a novel form of cerebellar hypoplasia/atrophy with early motor neuronopathy. Neuromuscul. Disord. 27, S176-S177.

Garcia-Esparcia, P., et al., 2017. Altered mechanisms of protein synthesis in frontal cortex in Alzheimer disease and a mouse model. American Journal of Neurodegenerative Disease 6(2), 15-25.

Iacono, G., et al., 2017. Integrated transcriptional analysis unveils the dynamics of cellular differentiation in the developing mouse hippocampus. Sci. Rep. 7(1), 18073.

Katsumata, Y., et al., 2017. Gene-based association study of genes linked to hippocampal sclerosis of aging neuropathology: GRN, TMEM106B, ABCC9, and KCNMB2. Neurobiol. Aging 53, 193 e117-193 e125.

Komine, Y., et al., 2006. Novel transcription factor zfh-5 is negatively regulated by its own antisense RNA in mouse brain. Mol. Cell. Neurosci. 31(2), 273-283.

Komine, Y., et al., 2012. Behavioral abnormalities observed in Zfhx2-deficient mice. PLoS One 7(12), e53114.

Kysenius, K., et al., 2012. PCSK9 regulates neuronal apoptosis by adjusting ApoER2 levels and signaling. Cell. Mol. Life Sci. 69(11), 1903-1916.

Langerveld, A.J., et al., 2007. Gene expression changes in postmortem tissue from the rostral pons of multiple system atrophy patients. Mov. Disord. 22(6), 766-777.

Lencz, T., et al., 2010. Prediction of schizophrenia risk using homozygous genetic markers, in: Office, U.S.P.a.T. (Ed.). North Shore-Long Island Jewish Research Institute.

Liuzzi, J.P., et al., 2005. Interleukin-6 regulates the zinc transporter Zip14 in liver and contributes to the hypozincemia of the acute-phase response. Proc. Natl. Acad. Sci. U. S. A. 102(19), 6843-6848.

Martin, J., et al., 2014. Biological overlap of attention-deficit/hyperactivity disorder and autism spectrum disorder: evidence from copy number variants. J. Am. Acad. Child Adolesc. Psychiatry 53(7), 761-770 e726.

Meier, I., et al., 2010. Expression of the snoRNA host gene gas5 in the hippocampus is upregulated by age and psychogenic stress and correlates with reduced novelty-induced behavior in C57BL/6 mice. Hippocampus 20(9), 1027-1036.

Messaed, C., et al., 2007. Soluble expanded PABPN1 promotes cell death in oculopharyngeal muscular dystrophy. Neurobiol. Dis. 26(3), 546-557.

Padhi, B.K., et al., 2008. Gene expression profiling in rat cerebellum following in utero and lactational exposure to mixtures of methylmercury, polychlorinated biphenyls and organochlorine pesticides. Toxicol. Lett. 176(2), 93-103.

Parente, M.K., et al., 2012. Dysregulation of Gene Expression in a Lysosomal Storage Disease Varies between Brain Regions Implicating Unexpected Mechanisms of Neuropathology. PLoS One 7(3), e32419.
Peters, J.L., et al., 2007. Targeting of the mouse Slc39a2 (Zip2) gene reveals highly cell-specific patterns of expression, and unique functions in zinc, iron, and calcium homeostasis. Genesis 45(6), 339-352.
Poirier, S., et al., 2006. Implication of the proprotein convertase NARC-1/PCSK9 in the development of the nervous system. J. Neurochem. 98(3), 838-850.
Rafalski, V.A., et al., 2013. Expansion of oligodendrocyte progenitor cells following SIRT1 inactivation in the adult brain. Nat. Cell Biol. 15(6), 614-624.
Riva, N., et al., 2016. Unraveling gene expression profiles in peripheral motor nerve from amyotrophic lateral sclerosis patients: insights into pathogenesis. Sci. Rep. 6, 39297.
Rousselet, E., et al., 2011. PCSK9 reduces the protein levels of the LDL receptor in mouse brain during development and after ischemic stroke. J. Lipid Res. 52(7), 1383-1391.
Seidah, N.G., et al., 2003. The secretory proprotein convertase neural apoptosis-regulated convertase 1 (NARC-1): liver regeneration and neuronal differentiation. Proc. Natl. Acad. Sci. U. S. A. 100(3), 928-933.
Sun, D., et al., 2017. LncRNA GAS5 inhibits microglial M2 polarization and exacerbates demyelination. EMBO Reports 18(10), 1801-1816.
Tajouri, L., et al., 2003. Quantitative and qualitative changes in gene expression patterns characterize the activity of plaques in multiple sclerosis. Brain Res. Mol. Brain Res. 119(2), 170-183.
Taoka, M., et al., 1992. A rat cerebellar protein containing the cdc10/SWI6 motif. Eur. J. Biochem. 207(2), 615-620.
Zhao, R.B., et al., 2018. GAS5 silencing protects against hypoxia/ischemia-induced neonatal brain injury. Biochem. Biophys. Res. Commun. 497(1), 285-291.